Rare Metal Materials and Engineering
Volume 46, Issue 6, June 2017
Online English edition of the Chinese language journal

Available online at www.sciencedirect.com
ScienceDirect

Cite this article as: Rare Metal Materials and Engineering, 2017, 46(6): 1474-1479.

ARTICLE

2D Model and 3D Reconstitution of Sintered Metal Fibers by Surface Diffusion

Chen Dongdong[1], Zheng Zhoushun[1], Wang Jianzhong[2], Tang Huiping[2]

[1] Central South University, Changsha 410083, China; [2] State Key Laboratory of Porous Metal Materials, Northwest Institute for Nonferrous Metal Research, Xi'an 710016, China

Abstract: According to the sections of sintered junction of two metal fibers, which are oval-oval geometry structure in different directions, an oval-oval model was developed based on the traditional surface diffusion mathematical model. This model was numerically solved by a level set method to achieve the 2D simulations of two sintered metal fibers. Moreover, the 3D reconstitution method was proposed to depict the complex 3D geometrical structure of sintered junction. The 2D simulations and 3D reconstitution results of two metal fibers with the fiber angle 30 °well agree with the experimental ones, which imply that the 2D model and 3D reconstitution method are correct. In addition, the numerical simulation results show that the growth rate of sintered neck along the directions taken from the bisector of obtuse angle to the bisector of acute angle is increased.

Key words: 2D model; 3D reconstitution; metal fiber; sintered neck; surface diffusion

Porous metal fiber materials are the third generation porous metal materials. Due to their filtration separation, energy absorption, sound absorption, efficient combustion, enhanced heat and mass transfer, the porous metal fiber materials have been widely used in the fields of electronics, chemicals, textiles, machinery, food and medicine[1-3].

Previously, researchers have carried out some work on the sintering mechanism of the porous metal fiber materials. In the 1960s, Pranatis et al.[4] studied the sintering mechanism of metal fibers and found the significant difference about sintering mechanism between metal fiber and metal powder. The main sintering mechanism of the metal powder is surface diffusion, while that of metal fiber is the combined action of surface diffusion and volume diffusion. Bal'shin et al.[5] investigated the sintering shrinkage of metal fiber, and found the elastic strain energy of metal fiber could strongly affect the process of sintering shrinkage. Kostornov et al.[6-8] systematically studied the sintering process of metal fiber with different materials and wire diameters. In addition, he studied the sintering mechanism of metal fiber according to the theory of viscous flow of sintered metal powder. Recently, some researchers focused on the preparation and application of the porous metal fiber materials[9-11]. Tang et al.[12] studied the sound absorbing properties of stainless steel fiber porous materials, and found that the sound absorption coefficient increases with increasing porosity and thickness of fibrous materials. Wang et al.[13] studied the fractal dimension for porous metal materials of FeCrAl fiber, and found that the fractal dimension decreases with the increase of the magnification and increases continuously with enhancing the porosity. Zhou et al.[14] established both three- and four-point bending setup to characterize the bending properties of porous metal fiber sintered sheet, and found that both three- and four-point bending strength were decreased with increasing porosity ranging from 70% to 90% and higher sintering temperature produced higher bending strength for the porous metal fiber sintered sheet sintered in the temperature range of 700~1000 ℃. Xu et al.[15] studied the consolidation process of SiCf/Ti-6Al-4V composites by matrix-coated

Received date: June 14, 2016
Foundation item: National Natural Science Foundation of China (51174236, 51134003); National Key Basic Research Development Program of China ("973" Program) (2011CB606306); Opening Project of State Key Laboratory of Porous Metal Materials (PMM-SKL-4-2012)
Corresponding author: Zheng Zhoushun, Ph. D., Professor, School of Mathematics and Statistics, Central South University, Changsha 410083, P. R. China, E-mail: zszheng@csu.edu.cn

fiber method via hot pressing using finite element modeling, and found that the higher fiber content will lower the consolidation rate.

However, the studies on the formation of sintered neck of metal fibers does not make a breakthrough. Generally, the studies on metal fiber are mainly based on metal powder sintering theory. Unlike the completely symmetrical shape of metal powder, which can be characterized by ball-ball model or ball-plate model in two-dimensional space[16], the shape of metal fibers is very complex in three-dimensional space. Therefore, the metal fiber is represented by a cylinder to investigate the formation of sintered neck.

In this study, based on the traditional surface diffusion model[17, 18], the 2D model of sintered metal fiber, which is called oval-oval model, will be developed to simulate the growth process of sintered neck with the fiber angle of 30° in every section. The 3D reconstitution method will be proposed to achieve the 3D simulation of sintered metal fiber. The growth rate of sintered neck in different sections will be investigated by the numerical simulation results.

1 Surface Diffusion Model and Level Set Method

1.1 Surface diffusion model

Surface diffusion results in mass flow along the fiber surface and hence changes surface morphology[17]. Mass flow is generated by the surface chemical potential gradient which is proportional to the surface curvature. Hence, the surface flux is the result of the diffusion coefficient and the surface gradient of the curvature. Then the velocity of the surface normal to itself is proportional to the divergence of the surface flux, which is the Laplacian of the curvature[18,19]. Therefore, the mathematical model describing the surface movement introduced by Mullins[20] can be expressed as,

$$\frac{\partial r_{\mathrm{n}}}{\partial t}=B\frac{\partial^2 K}{\partial s^2} \tag{1}$$

where r_{n} is the normal vector of the surface, t represents time, K is the surface curvature, s is the arc length and B is a coefficient defined by

$$B=\frac{\delta_{\mathrm{s}}D_{\mathrm{s}}\gamma\Omega}{kT} \tag{2}$$

where D_{s} is the surface diffusion coefficient, γ is the surface free energy per unit area, Ω represents the atomic volume, δ_{s} is the surface diffusive width, k is the Boltzmann's constant and T is the absolute temperature.

1.2 Level set method

The mathematical model developed by Mullins can be solved by method of lines[18] or finite difference method[19]. The main advantage of these methods is the straightforward interface definition. However, its main disadvantage is that they are difficult to capture topological changes. In this paper, the level set method was used to solve the mathematical model. Level Set method was proposed by Osher and Sethian[21] and further developed during the past several years. The method can be used to capture the interface rather than track it and makes it possible to capture drastic changes in the shape of curves and even topology changes. In addition, the method is stable, and the equations are not unnecessarily stiff and geometric quantities, so that the curvature can be computed easily[22-25].

The basic idea of the method is embedding the interface into a higher dimensional space. Considering a closed moving interface $\Gamma(t)$ in R^2, let $\Omega(t)$ be the region that is enclosed by $\Gamma(t)$. The auxiliary function is $\phi(x,y,t)$, which is called the level set function, and this function is Lipchitz continuous and satisfies the following conditions:

$$\begin{cases}\phi(x,y,t)<0, \text{ in } \Omega(t)\\ \phi(x,y,t)=0, \text{ on } \Gamma(t)\\ \phi(x,y,t)>0, \text{ in } R^2\setminus\overline{\Omega(t)}\end{cases} \tag{3}$$

Conversely, if $\phi(x,y,t)$ is known, the interface can be located by finding the zero level set of $\phi(x,y,t)$. That is, $\Gamma(t)=\{x:\phi(x,y,t)=0\}$. So moving the interface is equivalent to updating $\phi(x,y,t)$, which can be done by solving a Hamilton-Jacobi-type equation.

The Hamilton-Jacobi-type equation has the form,

$$\begin{cases}\phi_t+H(\phi_x,\phi_y)=0\\ \phi(x,y,0)=\phi_0(x,y)\end{cases} \tag{4}$$

If $H(\phi_x,\phi_y)=F|\nabla\phi|$, Eq.(4) is the evolution function. The normal velocity F is considered to be a function of spatial derivatives of $\phi(x,y,t)$. In many applications, F is a function of the curvature K and its spatial derivatives. The curvature can be computed via the level set function $\phi(x,y,t)$ as,

$$K=\nabla\cdot n$$

$$n=\frac{\nabla\phi}{|\nabla\phi|}=\left(\frac{\phi_x}{\left(\phi_x^2+\phi_y^2\right)^{\frac{1}{2}}},\frac{\phi_y}{\left(\phi_x^2+\phi_y^2\right)^{\frac{1}{2}}}\right) \tag{5}$$

Here n is the normal vector which coincides with the unit normal vector for the surface on zero level set. According to Eq. (5), the expression of K can be expressed as:

$$K=\nabla\cdot\frac{\nabla\phi}{|\nabla\phi|}=\frac{\phi_{xx}\phi_y^2-2\phi_x\phi_y\phi_{xy}+\phi_{yy}\phi_x^2}{(\phi_x^2+\phi_y^2)^{\frac{3}{2}}} \tag{6}$$

In the case of surface diffusion,

$$F=-B\frac{\partial^2 K}{\partial s^2} \tag{7}$$

The second order derivative of curvature can be expressed as:

$$\begin{aligned}\frac{\partial^2 K}{\partial s^2}&=\nabla\left[\nabla K\cdot\frac{(\phi_y,-\phi_x)}{|\nabla\phi|}\right]\cdot\frac{(\phi_y,-\phi_x)}{|\nabla\phi|}\\ &=\frac{K_{xx}\phi_y^2-2K_{xy}\phi_x\phi_y+K_{yy}\phi_x^2}{\phi_x^2+\phi_y^2}-\frac{K(K_x\phi_x+K_y\phi_y)}{\sqrt{\phi_x^2+\phi_y^2}}\end{aligned} \tag{8}$$

The second order derivative of curvature is a nonlinear term

involving fourth order derivative of function ϕ.

2 Oval-oval Model Established by Level Set Method

2.1 Oval-oval model

In Fig.1, it is assumed that the fiber angle is β, and the bisector of obtuse angle represents polar axis. The polar coordinate system is established by rotating the polar axis counterclockwise, and α represents the angle in polar coordinates. The sections of the sintered junction are taken from every direction, and they may be circular, oval and rectangular. In Fig.2, Cartesian coordinates system is established in the cross section, and O_1 represents the oval in the above, O_2 represents the oval under O_1, O_3 represents the circle which is tangent to O_1 and O_2 simultaneously. ρ is the radius of O_3, a is the radius of metal fiber and r is the length of sintered neck.

According to the geometric relationship shown in Fig.1 and Fig.2, the functions of O_1 and O_2 can be expressed as:

$$O_1: \quad \frac{x^2}{a^2}\cos^2\left(\frac{\beta}{2}-\alpha\right)+\frac{(y-a)^2}{a^2}=1 \tag{9}$$

$$O_2: \quad \frac{x^2}{a^2}\cos^2\left(\frac{\beta}{2}+\alpha\right)+\frac{(y+a)^2}{a^2}=1 \tag{10}$$

where the change of α ($0\le\alpha\le\pi$) describes the cross section in every direction.

It is assumed that surface diffusion is responsible for surface movement. Then the velocity of the surface normal to itself is proportional to the divergence of the surface flux, which is the Laplacian of the curvature. The implicit function $\phi(x,y,t)$ represents the interface and its changes make the interface evolve. In order to define the evolution of the function $\phi(x,y,t)$, the evolution equation can be expressed as,

$$\phi = F\left|\nabla\phi\right|, \quad \text{given } \phi(x,y,t=0) \tag{11}$$

where $F=-B\dfrac{\partial^2 K}{\partial s^2}$. This is coincided with Eq.(1).

For each cross section, the level set function is defined as:

$$\begin{cases}\phi(x,y,t)<0, & \text{in } \Omega(t)\\ \phi(x,y,t)=0, & \text{on } \Gamma(t)\\ \phi(x,y,t)>0, & \text{in } R^2\setminus\overline{\Omega(t)}\end{cases} \tag{12}$$

where $\Gamma(t)$ is the curve (interface) determined by Eq.(9) and Eq.(10), and $\Omega(t)$ represents the inner region surrounded by interface, as shown in Fig.3.

Based on the oval-oval model proposed above, the algorithm to solve this model is similar to what proposed in Ref.[24].

2.2 3D reconstitution

The oval-oval model is solved by level set method to obtain the evolution of the interfaces in different directions, and then the 3D geometry structure of sintered neck is established by reconstituting these interfaces.

The process of 3D reconstitution is expressed as follows:

Step 1. Extract the position coordinates of interface $\Gamma(t)$. According to the 2D numerical simulation results in every section, the position coordinates of interface, which are expressed as (x',y'), can be extracted from these sections.

Step 2. Coordinate transformation. According to the coordinates obtained from Step 1, these coordinates can be transformed to 3D coordinates (x,y,z). The coordinate transformation formulation can be expressed as follows:

$$\begin{cases}x=x'\cos\alpha\\ y=x'\sin\alpha\\ z=y'\end{cases}$$

where α represents the angle in polar coordinates.

Step 3. Plot 3D figure. According to the 3D coordinates obtained from Step 2, the sections can be plotted in a 3D figure. The 3D geometry structure can be reconstituted when all sections are plotted in the 3D figure.

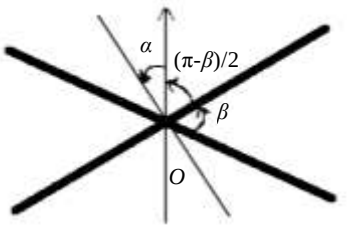

Fig.1 System of polar coordinates

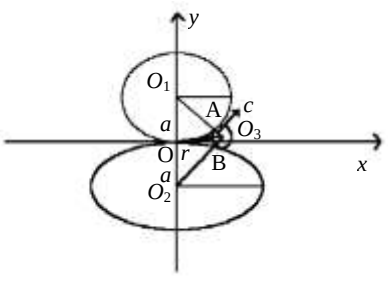

Fig.2 Section of two metal fibers

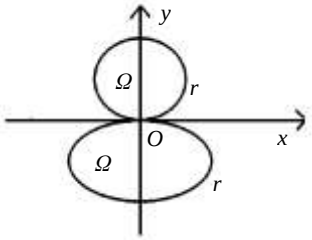

Fig.3 Internal area and interface of the cross section

3 Numerical Simulation Results and Comparisons

The growth process of sintered neck of two metal fibers with the fiber angle of 30 ° is simulated by surface diffusion. The speed function of curve evolution is $F=-B\frac{\partial^2 K}{\partial s^2}$, where $B=1$. The 2D simulation and 3D reconstitution are implemented using Matlab. The meshing is 500×500, and $\Delta x=\Delta y=1$. The radius of metal fiber is 100.

3.1 Numerical simulation results

3.1.1 2D simulation result

Twelve sections are taken from the bisector of obtuse angle (α=0 °) to the bisector of obtuse angle on the other side (α=180 °) to compute. Actually, the sections taken from the bisector of obtuse angle to the bisector of acute angle (α=90 °) are rotational symmetry with the sections taken from the bisector of acute angle to the bisector of obtuse angle on the other side. Then the sections taken from the bisector of obtuse angle to the bisector of acute angle are shown in Fig.4. The step number of each figure is 1500, and the interface is marked every 300 steps.

3.1.2 3D simulation result

The 3D geometry structure is established by reconstituting the sections in different directions. When the evolution step number is 1000, the 3D geometry structure of two sintered metal fibers with the fiber angle of 30 ° is shown in Fig.5.

3.2 Comparisons with experimental results

The experimental results are shown in Fig. 6, which are the sections of sintered metal fibers with different fiber angles. Although the fiber angles are very difficult to determine exactly, comparing the numerical results (as shown in Fig. 4) with experimental ones (as shown in Fig. 6), it can be concluded that the numerical simulation results well agree with the experimental ones to some extent. Moreover, the 3D simulation result of two sintered metal fibers with the fiber angle of 30 ° (as shown in Fig. 5) well agree with the experimental ones (as shown in Fig.7).

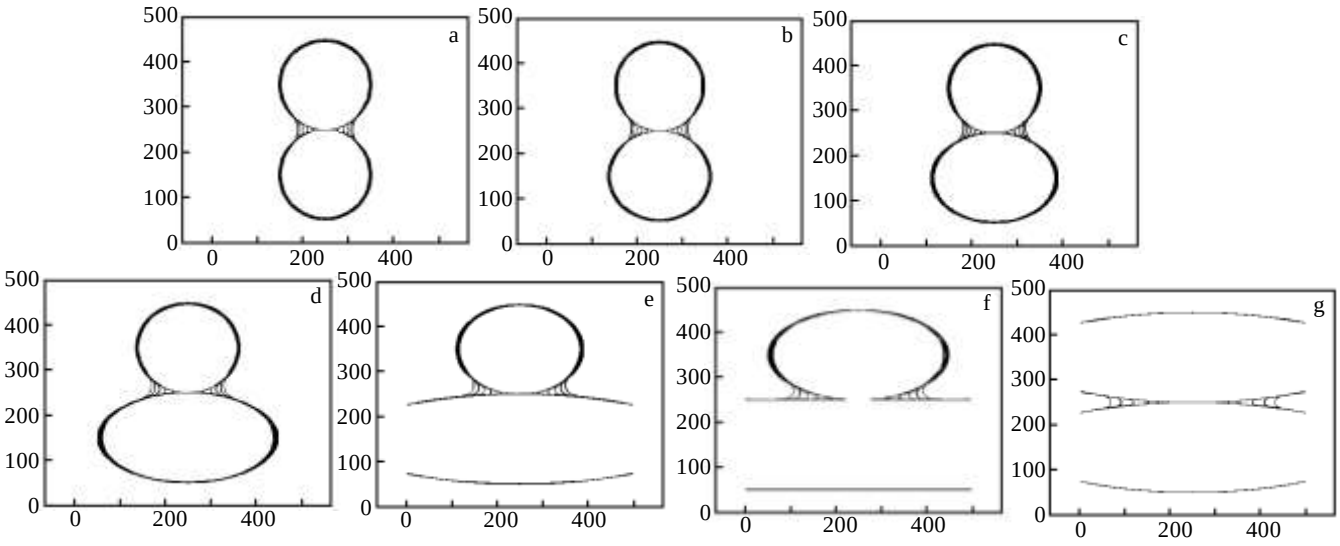

Fig.4 Section of two metal fibers with the fiber angle of 30 °: (a) α=0 ° (the section in the direction of the bisector of obtuse angle), (b) α=15 °, (c) α=30 °, (d) α=45 °, (e) α=60 °, (f) α=75 ° (the section in the direction of the nether fiber), (g) α=90 ° (the section in the direction of the bisector of acute angle)

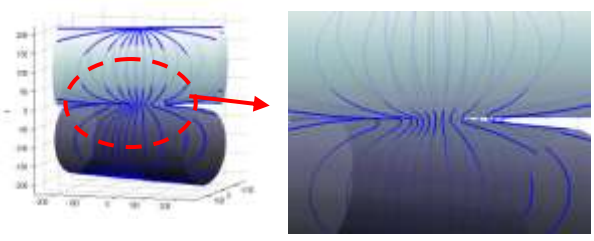

Fig. 5 Reconstructed 3D geometry structure of two sintered metal fibers with the fiber angle of 30 °

4 Discussions

For two metal fibers with the fiber angle 30 °, the sintered neck radius is plotted as a function of time in Fig. 8. The growth trend of neck radius along seven directions (from the bisector of obtuse angle to the bisector of acute angle) is same. In the initial stage of sintering, the growth rate of sintered neck is fast and the sintered neck radius almost grows linearly with the time extending. When the time t exceeds 30, the growth rate slows down gradually, and

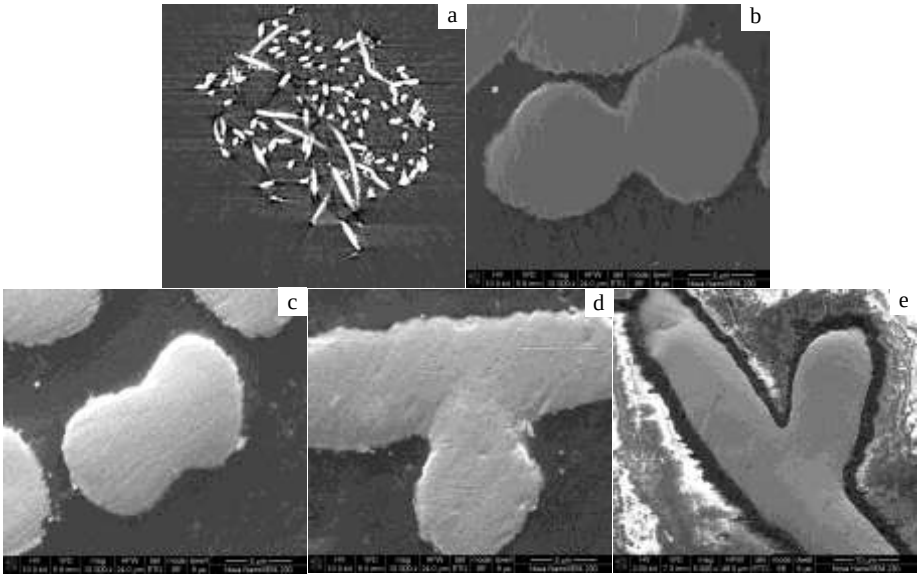

Fig. 6 Sections morphology of sintered metal fibers (a) and corresponding high magnification morphologies (b~e)

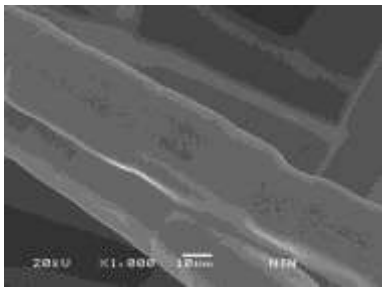

Fig. 7 Sintered neck of two metal fibers with the fiber angle of 30 °

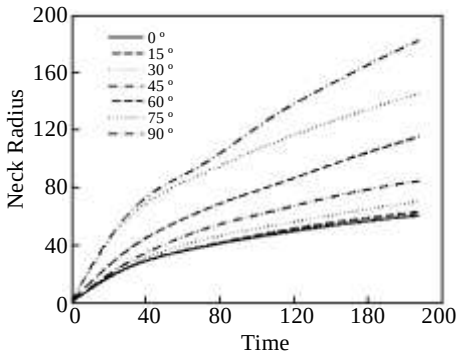

Fig. 8 Sintered neck radius vs. time for metal fibers with the fiber angle of 30 °

it is close to 0. The neck radius along the bisector of acute angle is the largest; however, that along the bisector of obtuse angle is the smallest.

Based on the numerical simulation results shown in Fig. 4 and Fig.8, the growth rate of sintered neck along the directions taken from the bisector of obtuse angle to the bisector of acute angle $(0° \le \alpha \le 90°)$ is increased. Hence, it can be concluded that the closer to the bisector of acute angle the direction is, the faster the growth rate of sintered neck is, and the larger the sintered neck radius is. Also, the conclusion well agrees with the general experiment rule.

According to the analysis above, the simulations implemented by the 2D model and 3D reconstitution well agree with experimental results. Therefore, the 2D model and the corresponding numerical method are correct, and the 3D reconstitution method is reasonable.

5 Conclusions

1) Based on the traditional surface diffusion mathematical model, the oval-oval model is developed to achieve the 2D simulations of sintered metal fibers with the fiber angle 30 °.

2) In order to describe the sintering progress better, the level set method is adopted to solve the oval-oval model. The 3D geometrical structure of sintered neck of two metal fibers is very complex, which is not as simple as it of two metal powders.

3) The 3D reconstitution method is proposed to depict the complex 3D geometrical structure. The 2D numerical simulation results well agree with the experimental ones, and the 3D reconstitution result well depicts the geometrical structure. Therefore, the 2D model and the 3D reconstitution method are correct. In addition, according to the simulation results, the growth rate of sintered neck along the directions taken from the bisector of obtuse angle to the bisector of acute angle is increased.

References

1 Qiao Jichao, Xi Zhengping, Tang Huiping *et al. Rare Metal Materials and Engineering*[J], 2010, 39(3): 561 (in Chinese)
2 Ao Qingbo, Tang Huiping, Wang Jianzhong *et al. Rare Metal Materials and Engineering*[J], 2014, 43(10): 2344
3 Ao Qingbo, Tang Huiping, Zhu Jilei *et al. Rare Metal Materials and Engineering* [J], 2009, 38(10): 1765 (in Chinese)
4 Pranatis A L, Seigle L. *Proceedings of International Conference on Powder Metallurgy*[C]. New York: Interscience, 1961: 53
5 Bal'shin M Y, Rybal'chenko M K, Padalko O V *et al. Poroshkovaya Metallurgiya*[J], 1964, 3(3): 185
6 Kostornov A G, Akhmedov M K. *Poroshkovaya Metallurgiya*[J], 1993, 32(9): 110
7 Kostornov A G, Kirichenko O V, Brodikovskii N P *et al. Poroshkovaya Metallurgiya*[J], 2008, 47(9): 21
8 Kostornov A G, Kirichenko O V, Brodikovskii N P *et al. Poroshkovaya Metallurgiya*[J], 2008, 47(5): 39
9 Clynde T W, Markaki A E, Tan J C. *Composites Science and Technology*[J], 2005, 65(15): 2492
10 Jang H, Ko K, Kim S J *et al. J Wear*[J], 2004, 256(3): 406
11 Zhou Wei, Tang Yong, Wan Zhenping *et al. Transactions of Nonferrous Metals Society of China*[J], 2007, 17(5): 1028
12 Tang Huiping, Zhu Jilei, Wang Jianyong *et al. Transactions of Nonferrous Metals Society of China*[J], 2007, 17(12): 1943
13 Wang Jianzhong, Xi Zhengping, Tang Huiping *et al. Transactions of Nonferrous Metals Society of China*[J], 2013, 23(4): 1046
14 Zhou Wei, Wang Qinghui, Ling Weidong *et al. Materials and Design* [J], 2014, 56: 522
15 Xu Xianghong, Yang Yanqing, Luo Xian *et al. Rare Metals*[J], 2015, 34(12): 844
16 Guo Shiju. *The Theory of Sintered Metal Powder*[M]. Beijing: Metallurgical Industry Press, 1998:15 (in Chinese)
17 Zhang Wen, Ian Gladwell. *Computational Materials Science*[J], 1998, 12(2): 84
18 Zhang Wen, Schneibel J H. *Acta Metall Mater*[J], 1995, 43(12): 4377
19 German R M, Lathrop J F. *Journal of Materials Science*[J], 1978, 13(5): 921
20 Mullins W W. *J Appl Phys* [J], 1957, 28(3): 333
21 Osher S, Sethian J A. *J Comput Phys*[J], 1988, 79(1): 12
22 Osher S, Fedkiw R. *Level Set Methods and Dynamic Implicit Surfaces*[M]. New York: Springer-Verlag New YorkInc, 2003: 3
23 Sethian J A. *Commun Math Phys*[J], 1995, 101(4): 487
24 Khenner M, Averbuch A, Israeli M *et al. J Comput Phys*[J], 2001, 170(2): 764
25 Sethian J A. *Level Set Method: Evolving Interface in Geometry, Fluid Mechanics, Computer Vision and Materials Science*[M]. Cambridge: Cambridge University Press, 1996: 31

基于表面扩散机制金属纤维烧结的二维模型和三维重构

谌东东[1]，郑洲顺[1]，王建忠[2]，汤慧萍[2]

(1. 中南大学，湖南 长沙 410083)

(2. 西北有色金属研究院 金属多孔材料国家重点实验室，陕西 西安 710016)

摘 要：根据金属纤维烧结结点在不同方向的椭圆-椭圆结构，基于传统的表面扩散数学模型，建立了椭圆-椭圆模型。用水平集方法对模型进行数值求解，实现了金属纤维的二维模拟。此外，提出了三维重构方法描述烧结金属纤维复杂的三维几何结构。夹角为30°的 2 根金属纤维烧结的二维模拟和三维重构结果与实验结果相符，这说明本研究的二维模型和三维重构方法是正确的。另外，数值模拟结果表明：从 2 根金属纤维的钝角平分线方向到锐角平分线方向，烧结颈的生长速率增大。

关键词：二维模型；三维重构；金属纤维；烧结颈；表面扩散

作者简介：谌东东，男，1989 年生，硕士，中南大学数学与统计学院，湖南 长沙 410083， E-mail: cdd0525@163.com